frontiers in Earth Science

BRIEF RESEARCH REPORT
published: 07 April 2021
doi: 10.3389/feart.2021.641060

Histology and Geochemistry of *Allosaurus* (Dinosauria: Theropoda) From the Cleveland-Lloyd Dinosaur Quarry (Late Jurassic, Utah): Paleobiological Implications

Christophe Ferrante[1,2], Lionel Cavin[2], Torsten Vennemann[3] and Rossana Martini[1]*

[1] Department of Earth Sciences, University of Geneva, Genève, Switzerland, [2] Department of Geology and Palaeontology, Natural History Museum of Geneva, Genève, Switzerland, [3] Institute of Earth Surface Dynamics, University of Lausanne, Lausanne, Switzerland

The Late Jurassic *Allosaurus* is one of the better-studied dinosaurs. A histological and geochemical study of a tibia and a femur of *A. fragilis* recovered in the Upper Jurassic Cleveland-Lloyd Dinosaur Quarry, Utah, United States has been done in order to address growth characteristics of this species. The two bones, probably belonging to separate individuals, are among the largest known for this species, which make them suitable to address such issues. The inclusion of our data on femur growth markings in the previously published data reflects a range of growth variability rather than two distinct growth strategies. The tibia has a well-developed external fundamental system indicating somatic maturity achievement. Using a quantitative method of superimposition to retrocalculate missing lines of arrested growth, the tibia appears to correspond to an individual that reached its skeletal maturity at 22 years and died at approximately 26 years. In the tibia, the concentration of zinc, a potential biomarker associated with bone formation, displays a higher concentration in zones of rapid growth compared to annuli. There is no direct relationship between the values of $\delta^{18}O_p$ and the lines of arrested growth distribution. The absence of relations between the histological organization and an enrichment in REE of the bone, indicates that the variations of $\delta^{18}O_p$ likely represent a diagenetic process rather than a primordial, biologic composition. However, the geochemical composition of the bones is not homogeneous along the sections, indicating that the signal variations have not been completely erased by diagenesis.

Keywords: skeletal maturity, growth, tibia, femur, Morrison Formation

OPEN ACCESS

Edited by:
Martin Daniel Ezcurra, Museo Argentino de Ciencias Naturales Bernardino Rivadavia, Argentina

Reviewed by:
Christopher Griffin, Yale University, United States
Michael D'Emic, Adelphi University, United States

****Correspondence:***
Lionel Cavin
lionel.cavin@ville-ge.ch

Specialty section:
This article was submitted to Paleontology, a section of the journal Frontiers in Earth Science

Received: *13 December 2020*
Accepted: *17 March 2021*
Published: *07 April 2021*

Citation:
Ferrante C, Cavin L, Vennemann T and Martini R (2021) Histology and Geochemistry of Allosaurus (Dinosauria: Theropoda) From the Cleveland-Lloyd Dinosaur Quarry (Late Jurassic, Utah): Paleobiological Implications. Front. Earth Sci. 9:641060. doi: 10.3389/feart.2021.641060

INTRODUCTION

Bone paleohistology, in particular skeletochronology, is a predominant method for reconstructing the life history of extinct vertebrates (e.g., Prondvai, 2017). Due to their phylogenetic proximity to birds and their still uncertain physiology, non-avian dinosaurs are the subject of numerous histological studies aiming at determining life traits, such as growth rate or sexual maturity.

Combined with this approach, geochemical analyses make it possible to explore the behavioral and environmental characteristics of non-avian dinosaurs, in particular via the stable oxygen isotope composition (e.g., Tütken et al., 2004).

Allosaurus is one of the best-known theropod taxa (Chure and Loewen, 2020; Evers et al., 2020), and remains of this genus are particularly abundant in the Cleveland-Lloyd Dinosaur Quarry (CLDQ, Utah, United States) with up to 46 individuals identified based on the occurrence of 46 left femora (Madsen, 1976; Gates, 2005). The abundance of fossil material has stimulated much work on the osteology, growth strategy, ontogeny and histology of this dinosaur (e.g., Madsen, 1976; Reid, 1996; Smith, 1998; Bybee et al., 2006; Lee and Werning, 2008). To assess the growth strategy of *Allosaurus*, Bybee et al. (2006) estimated, on the basis of histological analyses of the largest individuals of the CLDQ, that skeletal maturity is reached between 13 and 19 years with a maximum growth rate at 15 ± 2 years. However, they did not find evidence of an External Fundamental System (EFS), indicating stabilization of growth, although an incipient EFS has been reported from an isolated and fragmentary *Allosaurus* fibula (UUVP 6346). They also estimate that the upper age limit is between 22 and 28 years. By counting lines of arrested growth (LAGs) and performing growth curve reconstructions, Lee and Werning (2008) estimated that *Allosaurus* was reproductively mature at 10 years. Bybee et al. (2006) and Prondvai (2017) showed a wide range of intraspecific variation in growth strategies in *Allosaurus fragilis*.

The Natural History Museum of Geneva, Switzerland houses a composite and partial skeleton of *Allosaurus fragilis* from CLDQ (Madsen, 1976). The tibia of this compound specimen is one of the longest tibiae recovered from this locality, making it a valuable specimen for tackling the question of growth strategy and age of skeletal maturity. We analyzed the isotopic composition of oxygen in order to investigate possible relationships between the $\delta^{18}O_p$ values and the histological pattern that would reflect biological or environmental signals (e.g., Tütken et al., 2004; Eagle et al., 2011), and also the rare earth elements to assess the impact of the diagenetic process on this bone. Similar analyses were made for comparison on a femur, which also belongs to a large individual but without evidence that it belong to the same individual with the tibia. The study of these bones corresponding to large individuals makes it possible to test for the presence of an EFS and of a determined growth, and to expand the data set to address the growth strategy of this species.

MATERIALS AND METHODS

Geological and Paleoenvironmental Settings

CLDQ is located in the Brushy Basin Member of the Morrison Formation (Hunt et al., 2006). The site is Late Jurassic in age (late Kimmeridgian-Tithonian). Two samples of an ash bed at 0.5–1 meters above the fossil bed gave K-Ar age estimates of 146.8 and 147.2 Ma (Kowallis et al., 1998; Bilbey, 1999). It should be noted that recalibration of former $^{40}Ar/^{39}Ar$ datings from the Morrison Formation (but not of the two samples mentioned above) gave ages of about two Ma older than the original datings (Trujillo and Kowallis, 2015). Bones occur in a calcareous mudstone, which is the main bone-bearing deposit, and in the overlying limestone (Gates, 2005). The mudstones and limestones of the CLDQ have been deposited in a lacustrine environment (Hunt et al., 2006). However, several environmental and taphonomic interpretations have been proposed such as an oxbow (Dodson et al., 1980), a floodplain pond in an anastomosing system (Richmond and Morris, 1996), a spring-fed pond or seep (Bilbey, 1999) and ephemeral pond (Gates, 2005; Peterson et al., 2017). Paleoclimatic reconstructions of the Morrison Formation indicate that the climate was warm and strongly seasonal (e.g., Dodson et al., 1980; Turner and Peterson, 2004; Tanner et al., 2014), i.e., a more or less dry season followed by a humid season characterized by monsoonal conditions.

Bone Specimens

The analyzed bones are part of a composite skeleton of *Allosaurus fragilis* (MHNG GEPI V2567) housed in the Natural History Museum of Geneva (Madsen, 1976). This material was collected in the CLDQ during the excavation campaign of 1962 directed by James Madsen and then offered by the Women's club of Utah in the seventies to the Geneva Museum.

Previous work pointed out that the midshaft of long bones best preserves the ontogenic record compared to other parts of the bones (Chinsamy-Turan, 2005; Padian and Lamm, 2013). Because histological and geochemical analyses are destructive methods, we selected two broken limb bones, a right femur and a right tibia (**Figure 1**). The selection of bones from CLDQ for the more than 50 composite skeletons containing a varying number of original bones sent to various institutions, including the composite skeleton with the femur and tibia studied here, was based on the selection of corresponding isolated bones to individuals of similar size (Madsen, 1976). Therefore, the fact that the femur and tibia correspond to animals of similar size is a weak indication that they belong to a single individual. In addition, the different histological patterns observed in the two bones (see below) do not allow attributing the two ossifications to a single individual on the basis of ontogenetic histological stages, annual cyclicity, growth marks, remodeling rate and the number of generations of secondary osteons as proposed by Wiersma-Weyand et al. (2021). Therefore, we have no evidence that both bones belong to the same individual. The femur (MHNG GEPI V2567a) consists of the half-distal part, which is broken into three fragments. The preserved length of the bone is 390 mm long and its circumference at the level of the sample measures 309 mm. Reconstruction of the complete bone by comparison with a complete femur illustrated by Madson (1976: plate 50) indicated that it measured approximately 792 mm in total length, making it a large femur for this species although not the largest known one. A 28 × 37 mm sample for histological and geochemical analyses was sawn out of the midshaft, approximately at 7/10 of the total length of the bone from the proximal end (**Figure 1A**). The tibia (MHNG GEPI V2567b), better preserved than the femur, is complete and measures 747 mm in length with a circumference of 275 mm at its midshaft (**Figure 1B**), making it the largest one among the set measured by Madsen (1976).

A 30 × 18 mm sample for histological and geochemical analyses was sawn out of the midshaft, approximately at half of the length of the bone (**Figure 1B**).

Geochemical Analyses

Preparations and analyses of the major and trace element as well as the isotopic compositions were done in the laboratories of the University of Lausanne (Switzerland). Samples were taken from broken surfaces of the bones that were refreshed by polishing in order to avoid surface contamination. Powder samples were scraped off perpendicular to the radial direction of growth using a hand-operated Proxxon Mini-drill equipped with a 1 mm diameter diamond drill bit. Samples were then prepared for isotopic analysis following a modified small-amount silver phosphate precipitation procedure (after Kohn, personal communication and Dettman et al., 2001) (see **Supplementary Data**). Oxygen ($\delta^{18}O_p$) isotope compositions of phosphate and carbonate within phosphate (δ13C, $^{18}O_C$) were measured using a Thermal Conversion Elemental Analyzer (TCEA) at 1,450°C linked to a ThermoFinnigan Delta Plus XL gas source mass spectrometer. The composition of major (Ca, P) and trace elements (F, Cl) were analyzed using an electron microprobe, JEOL 8200 Superprobe. REE (La to Lu) and some other major (Na, Mg, Al, Ti, Mn, Fe) and trace (V, Cu, Zn, Rb, Sr, Y, Zr, Nb, Cs, Ba, Pb, Th, U, Sc) elements were analyzed using laser ablation with inductively coupled plasma ion source mass-spectrometry (LA-ICP-MS). These two last analyses were made on polished and carbon coated (Superprobe) or decoated (LA-ICP-MS) thin sections of bones.

Histological Analyses

Thin sections of both tibia and femur were made from small blocks, extracted where the samples for geochemical analyses were also taken, using a hand-operated drill (Dremel), equipped with a rotary diamond wheel of 0.5 mm thick for a maximum bit of 15 mm. We sampled the bone blocks at the level of the natural breaks in the bones, i.e., roughly in the middle of the tibial shaft and in the distal third quarter of the femur because the bone is poorly preserved in its middle part (**Figure 1**). Polished thin sections were ground to a thickness of 80 μm. Thin sections were examined using transmitted normal- and polarized-light microscopy to identify histological structures.

Our equipment did not allow us to prepare a single thin section covering the entire section of the bone, making it not possible measuring the actual length of the LAGs. Therefore, we estimated the length of each LAG by assuming that they are equivalent to a circle with a radius corresponding to the LAG visible on the section. Comparison of the true length of the perimeter of the section of each bone (**Figure 1**, red circles) to the circle calculated with the radius on the corresponding outer rim (**Figure 1**, blue circles) indicated that the rim length is underestimated by 1% for the femur and 4.5% for the tibia. We considered that the margin of error is roughly similar for LAG length estimates, although the variation of the bone thickness around the medullary cavity makes a more detailed estimate difficult.

The age of the individuals was determined by counting the LAGs. The normal remodeling processes of growth and expansion of the medullary cavity have obliterated early growth records, so the missing LAGs were retrocalculated by aligning our length measurements in the graph of estimated age versus length circumference of LAGs provided by Bybee et al. for the bones of the limbs (2006: figure 2). In order to select the best fit of our data among several suboptimal visual alignments, we chose the one with the highest correlation coefficient when Bybee et al.'s data and our data are merged.

RESULTS

Histological Analyses

The femur and tibia differ substantially in their bone histology and also in their degree of remodeling (see **Supplementary Figures 1, 2** for higher resolution images of the histological

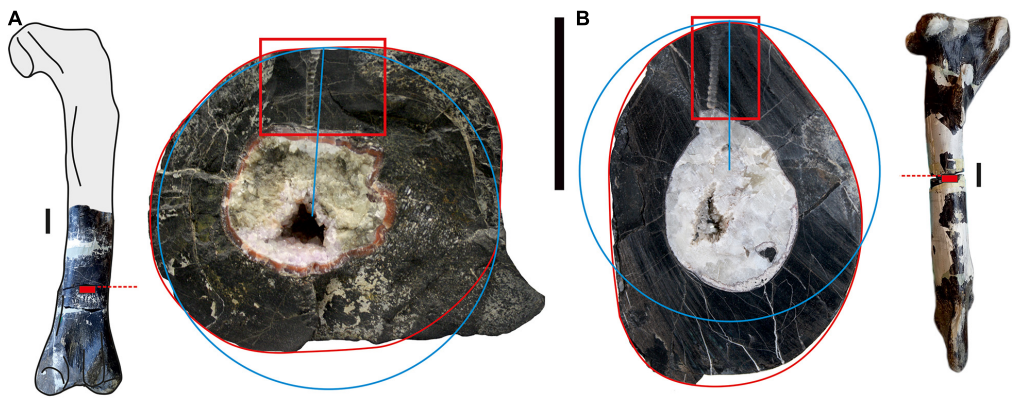

FIGURE 1 | (A) Right femur of *Allosaurus fragilis* (MHNG GEPI V2567a) in posterior view (missing part based on Madsen, 1976), location of the sample (red rectangle) and transverse section with the studied sample marked with red frame; **(B)** right tibia (MHNG GEPI V2567b) in lateral view, location of the sample (red rectangle) and transverse section with the studied sample marked with red frame. The blue circles correspond to the estimate of the length of the outer rim approximated as a circle compared to the actual length of the outer rim in red (see text for details). Scale bars equal 50 mm.

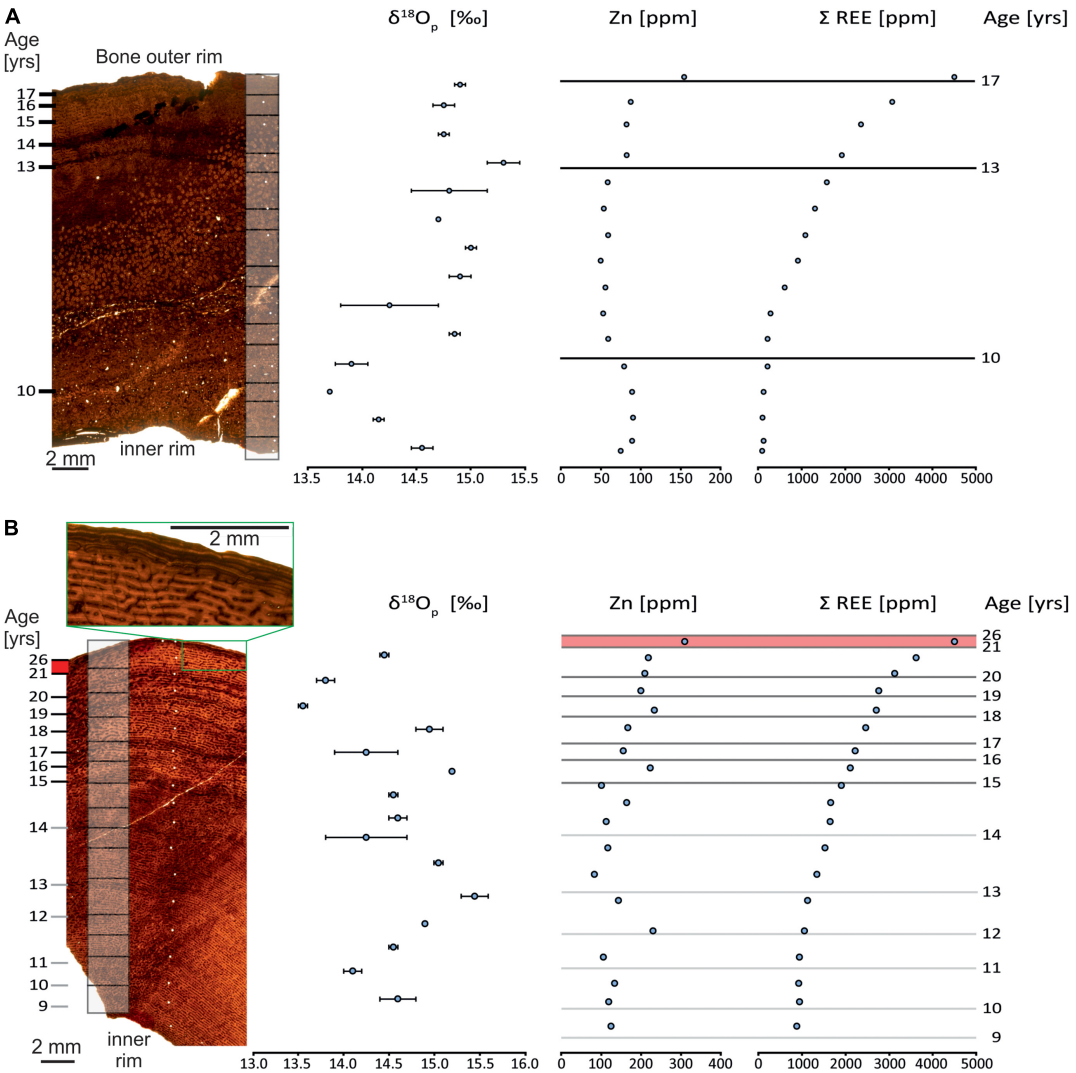

FIGURE 2 | Bone histology of the *Allosaurus fragilis* femur (MHNG GEPI V2567a) **(A)** and tibia (MHNG GEPI V2567b) **(B)** investigated for oxygen isotopic and geochemical composition. Gray boxes on the bone sections correspond to $\delta^{18}O_p$ sampling and white dots correspond to samples for LA-ICP-MS analyses; Dark lines on the graphs to the right correspond to visible LAG and grey lines correspond to the annuli. The green boxes in **(B)** frame the outer rim of the tibia with the EFS.

thin sections). The primary tissue of both bones are formed by fibrolamellar bone and were deposited as zonal bone tissue with cyclical growth marks (CGMs). Zonal bone tissue is composed of a zone and an annulus mostly accompanied by a LAG. Zones are thick, well vascularized and represent periods of fast bone deposition. In contrast, annuli are thin and denser than zones, less vascularized and deposited at a slower rate. LAGs represent a pause in osteogenesis (Chinsamy-Turan, 2005; Padian and Lamm, 2013).

The bone tissue of the femur (**Figure 2A**) is remodeled over its innermost two-thirds, displaying secondary osteons and well-developed and dense Haversian canals, possibly because the sample was taken relatively close to the bone distal end. The outermost cortex is made up of reticular fibrolamellar bone with cavities for blood vessels oriented linearly. About four marked cycles, with the alternation of zone, annulus and LAG are well preserved. One supplementary cycle is visible in the remodeled portion of the bone. No EFS is observed in the femur.

Unlike the femur, CGMs are visible throughout the sample of the tibia (**Figure 2B**), and are likely present over the entire section of the bone. Indeed, secondary remodeling with the formation of secondary osteons is only developed on small areas. Normal remodeling processes of growth and the expansion of the medullary cavity probably obliterated several of the internal most CGMs. Thirteen cyclical growth marks, each marked with a zone and an annulus, can be observed. The first six observable CGMs (**Figure 2B**, 9–14 years), though very poorly recorded and lacking a LAG, are still visible. The seven external CGMs (**Figure 2B**, 15–21 years) are mostly well-marked and all have a LAG. Bone tissue of the six first CGMs has small and linearly oriented canals for blood vessels, whereas they are larger and radially connected in the external better-marked CGMs. After the sixth cycle, which

points out the first LAG, the thickness of zones, and consequently the distance between the LAGs decreases, except for the last zone, which is thicker. The last zone is followed by about five closely spaced LAGs (**Figure 2B**), which is identified as an external fundamental system (EFS).

Major, Trace, and Rare Earth Elements

In situ microprobe investigations of the chemical composition indicate that the tibia and femur have mean F contents with of 3.71 wt.% (*SD* = 0.07, *n* = 15) and 3.72 wt.% (*SD* = 0.13, *n* = 14) (**Supplementary Table 1**), respectively, indicating that biogenic apatite of both bones is recrystallized into a homogenous carbonate-fluorapatite.

Along both bone profiles (**Supplementary Tables 1, 3–5**), major and trace element contents analyzed by electron-microprobe and LA-ICP-MS are either homogenous (CaO, P_2O_5, F, Na_2O, MnO, Cl, V, Zr, Nb, Ba, U), enriched at the outer rim with a decreasing trend toward the center (MgO, FeO, Al_2O_3, Sc, Cu, Sr, Y, Pb, Th) or present with a cyclical trend (Zn). Some trace elements that are otherwise homogeneous in concentration, may have strong punctual enrichments (Cu, Zr, Pb). The most external parts in both bones were excluded because they show obvious diagenetic enrichment.

LA-ICP-MS measurements (**Supplementary Table 5**) show that the tibia (**Figure 2B**) and femur (**Figure 2A**) are enriched in REE, in particular at the outer rim of the bone (**Figure 3**). The total REE content decreases inwards for both bones. These high values of REE are those typical for fossil bones older than the Cenozoic (Tütken et al., 2004). The tibia shows a total light REE enrichment of two orders of magnitude compared to the femur (**Figure 2**). However, the general trend is the same in both bones. Moreover, these results are similar to other analyses performed on fossils from other sites of the Morrison Formation as the CLDQ, the Howe Stephens Quarry and the Freeze out Hills (Suarez C. A., 2004; Herwartz et al., 2013).

Zinc has different concentration profiles in the two bones. In the tibia, it shows an irregular pattern (**Figure 2B**), in contrast to the femur, where it is less variable (**Figure 2A**). The tibia has a mean Zn content of 166 ppm with a maximum of 232 ppm and a minimum of 83 ppm with an irregular pattern (**Figure 2B** and **Supplementary Table 4**). In contrast, the femur has a mean Zn content of 76 ppm with a maximum of 91 ppm and a minimum of 49 ppm and presents a more regular pattern (**Figure 2A** and **Supplementary Table 4**).

Stable Isotope Compositions

The oxygen isotope compositions of the tibia and the femur have the same range in $\delta^{18}O_p$ values but the pattern of $\delta^{18}O_p$ values differ in each bone. The tibia (**Figure 2B** and **Supplementary Table 2**), which has multiple CGMs, has a mean $\delta^{18}O_p$ value of 14.6‰ (*SD* = 0.5‰, *n* = 15). The femur (**Figure 2A** and **Supplementary Table 2**), which is largely remodeled, has a mean $\delta 18O_p$ value of 14.6‰ (*SD* = 0.4, *n* = 14). The $\delta^{18}O_p$ values of both bones vary. This cyclic pattern is less marked in the femur compared to the tibia though. In the tibia, the length of the cycles of $\delta^{18}O_p$ values decreases toward the outside that is along the radial axis of growth. The amplitude of $\delta^{18}O_p$ cycles is similar though, with a maximum of 1.9‰. Zones have $\delta^{18}O_p$ values lower than those of annuli. In contrast, the $\delta^{18}O_p$ values of the femur have cycles of lower amplitude, with a maximum of 1.5‰ and more regularly spaced cycles. Furthermore, the $\delta^{18}O_p$ values are lower in the interior and higher in the exterior parts along the radial axis of growth. For both bones, the relatively coarse sample pattern hosen does not reveal a particular relationship between the values and the LAGs.

DISCUSSION

Paleoecological Implications of the Histological Data

Recently Prondvai (2017), suggested, on the basis of a dataset published by Lee and Werning (2008), that the growth trajectories of *A. fragilis* have a high range of intraspecific variations. However, she did not specify the bones that were sampled to reconstruct growth trajectories, and neither did Lee and Werning (2008). The raw data used in both studies was actually published by Bybee et al. (2006), an article not cited by Prondvai (2017). Bybee et al. provided regressions between estimates of age versus circumference of LAGs for several types of

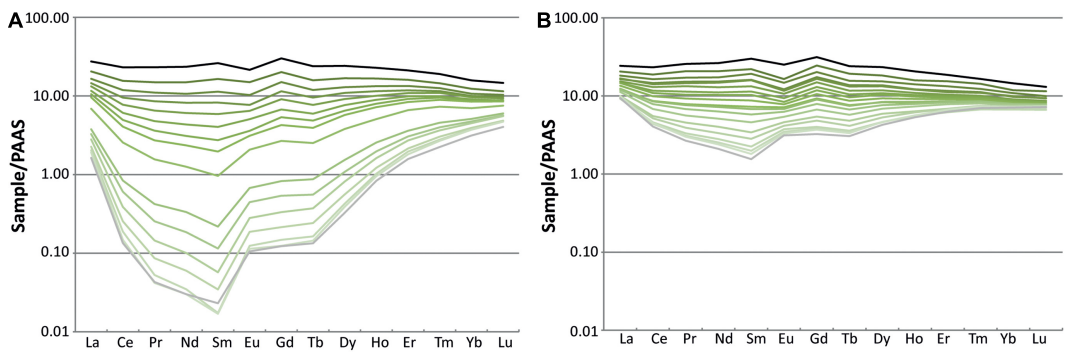

FIGURE 3 | REE patterns of the femur (MHNG GEPI V2567a) **(A)** and tibia (MHNG GEPI V2567b) **(B)** of *Allosaurus fragilis*. The black line represents LA-ICP-MS spot analyses at the outer bone rim, gray line those at the marrow cavity and shades of green lines represent analyses from the bone interior.

bone (femur, tibia, humerus, ulna), but they did not aggregate the points by individuals. Bybee et al. (2006) noticed a distinct double growth trajectory for the femora only, a variation also reported by Prondvai (2017) for the growth trajectories of *A. fragilis* in general. The values obtained here correspond to the strategy of "rapid growth" with a single individual (UUVP 3694) reaching a wider LAG circumference at a younger age (**Figure 4A**). Our **Figure 4**, however, illustrates that the strategy of "slow growth" is in fact represented by a single individual (UUVP 30-737), a situation not directly visible in Bybee et al.'s paper because individuals have not been identified in their figure (Bybee et al., 2006; **Figure 2**). In addition, the strategy of "rapid growth" is notably defined by a point abnormally high measured on the individual UUVP 3694 mentioned above. Other measurements of the circumference of the LAGs in this particular femur correspond well to the measurements obtained on the femur studied in the present work.

Therefore, because (1) the "slow growth strategy" is represented by a single individual in Babee et al. dataset and because (2) the "rapid growth strategy" is primarily based on a single, possibly outlier point that does not match the rest of the growth path relative to the femur path studied here, we consider the whole dataset to reflect a range of the growth variation rather than two distinct growth strategies. This pattern resembles what is observed in the femurs of the sauropodomorph *Plateosaurus* (Sander and Klein, 2005), indicating that the growth of *A. fragilis* was affected by environmental factors such as climate and availability of food. However, we recognize that even with the new data obtained here, the sample size remains small to draw solid conclusions and the interpretation of our graphical result with few dots can be misleading, as Gee et al. (2020) showed on the basis of a skeletochronology study of large sample of long bone from a Permian lissamphibian.

Seven LAGs are observed in the studied tibia (**Figure 2B**). By computing them after the circumference-to-age regression of Bybee et al. (2006), it appears that the expansion of the medullary cavity and normal remodeling had removed at least the fourteen first LAGs (**Figure 4B**). The EFS started to be deposited when the individuals reached about 22 years of age. The EFS contains about five LAGs indicating that this specimen lived at least 5 years after reaching its skeletal maturity. Consequently, by summing observable (7 LAGs), retrocalculated (14 LAGs) and LAGs composing the EFS (5 LAGs), the individual represented by the tibia possibly reached an age of 26 years (**Figures 2B**, **4B**). These results correspond approximately to the age limit calculated by Bybee et al. (2006), who estimated that skeletal maturity is reached between 13 and 19 years and that the upper age limit is between 22 and 28 years. The presence of an EFS supports the fact that *Allosaurus* has a determinate growth strategy as previously supposed (Bybee et al., 2006). The only report of an incipient EFS was from an isolated fragment of an *Allosaurus* fibula EFS (UUVP6346, Bybee et al., 2006). In other theropods, skeletal maturity probably began at about 18.5 years in *Tyrannosaurus* and between 14 and 16 years in *Albertosaurus* and *Daspletosaurus* (Erickson et al., 2004). The occurrence of an EFS in *Allosaurus* is not surprising. Such structure is reported for various archosaurs such as Pseudosuchia, Crocodylomorpha, Pterosauria and Dinosauria (Andrade et al., 2015). Among theropod dinosaurs, EFS were identified in *Tyrannosaurus*, *Albertosaurus*, *Daspletosaurus* (Erickson et al., 2004), *Masiakasaurus* (Lee and O'Connor, 2013), *Acrocanthosaurus* (D'Emic et al., 2012), *Troodon*, *Citipati,* and *Oviraptor* (Erickson et al., 2007).

Oxygen Isotope Composition

It is important to estimate the degree of alteration of the geochemical compositions in order to assess if the data reflect a primary *in vivo* composition or a secondary alteration. Analysis of REE concentration is a way to test if the analyzed samples had experienced exchange with a diagenetic fluid, and consequently their degree of alteration (Tütken et al., 2004; Eagle et al., 2011; **Supplementary Data**).

REE contents of the biogenic apatite of the femur (**Figures 2A**, **3A**) and the tibia (**Figures 2B**, **3B**) are enriched in the outer parts, indicating that both bones are affected to an unknown degree by a secondary incorporation of REE during diagenesis. A study by Eagle et al. (2011, Supplementary Data), based on clumped isotope measurements of six teeth and three bone specimens of *Camarasaurus* sp. from the CLDQ concluded that all material from this site is altered as it has experienced heating during burial, which is in accordance with the local tectonic and diagenetic history of this region. However, the oxygen isotope compositions of the femur (**Figure 2A**) and the tibia (**Figure 3**) measured along the bone profile are not flat but show variations.

Therefore, the geochemical composition of the CLDQ fossil bones was not totally homogenized but was gradually altered toward the interior. All the oxygen isotope values may have been lowered from their original values. Accordingly, the *in vivo* $\delta^{18}O_p$ values may no longer be recorded and the small number of cycles, defined by the variations in relative changes in $\delta^{18}O_p$ values compared to the age estimated for the specimens, may indeed simply represent the cycles of diagenetic alteration. In any case, a larger number of analyses on a higher sampling density would be required to confirm the cyclicity in $^{\delta}$ $18O_p$ values.

Zinc: Potential Biomarker or Evidence of Non-biological Reworking?

Fossil material of the CLDQ is commonly found to be enriched in heavy metals, such as Mo, As, U, Pb, Sr, Mg, Na, and Zn (Peterson et al., 2017). This enrichment may either be through a diagenetic process, or part of a bioaccumulation during the decomposition of numerous dinosaur carcasses (Peterson et al., 2017). The water of the depositional environment corresponds to a neutral pH with possible fluvial influence (Suarez M. B., 2004), and was a reducing environment, as suggested by the presence of metal oxides, sulfides and barite (Peterson et al., 2017). In our study, only Zn appears to show a signal with a pattern associated to the microstructure of bone tissues. In the tibia (**Figure 2B**) the zinc pattern reveals higher concentrations within zones and lower in annuli. In the femur (**Figure 2A**), zinc concentration is more homogenous, but the reworked bone tissue with Haversian channels is enriched in zinc. Higher zinc concentrations in zones and in Haversian bone can be associated to faster growing bone

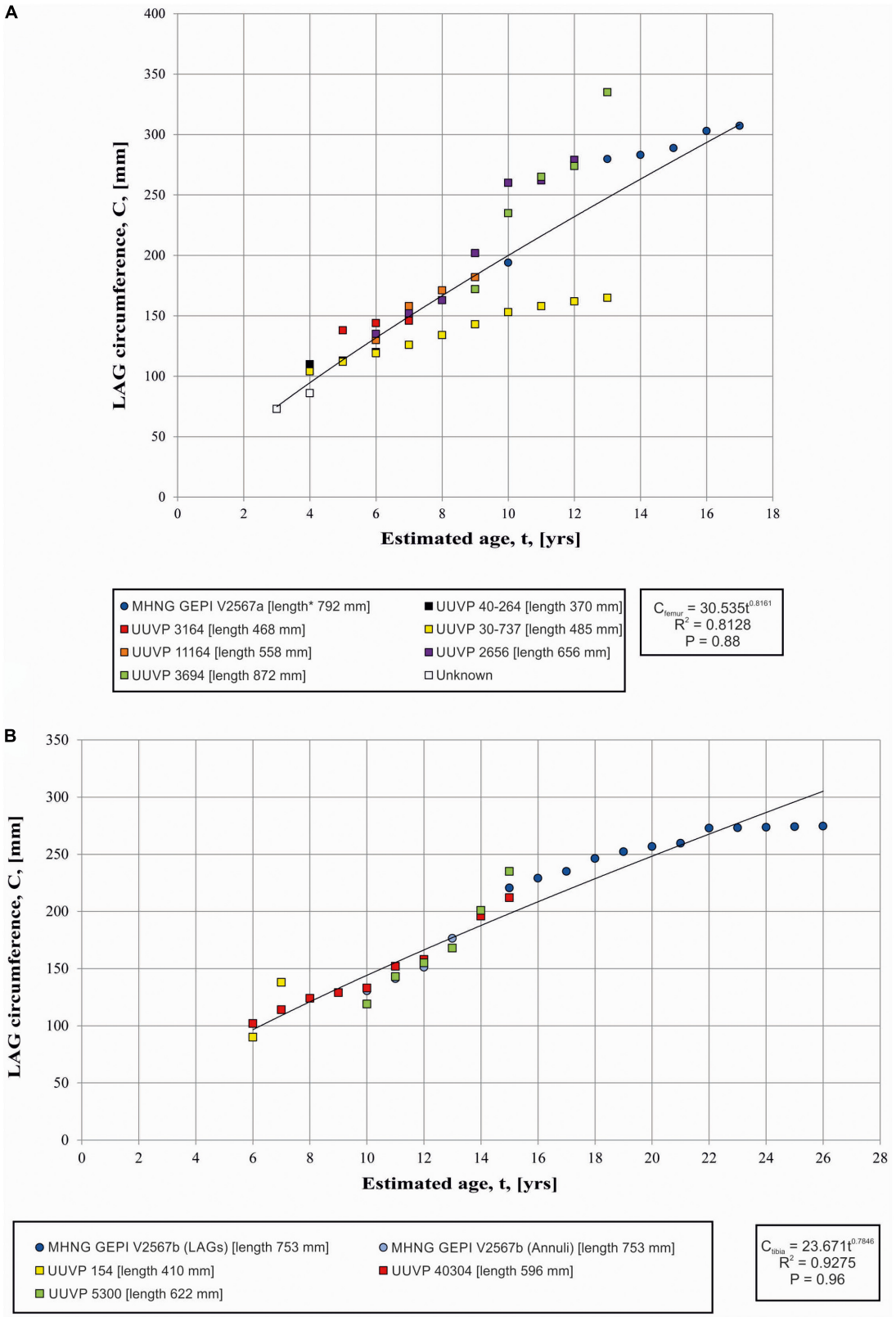

FIGURE 4 | (A) Variation of LAG circumferences and circumference-to-age regression in the femora **(A)** and Tibia **(B)** of *Allosaurus*. Squares refer to data from Bybee et al. (2006) and circles refer to the present study. * indicates the calculated length estimated by comparison with a complete specimen.

tissue and a faster reworking process. The measured zinc content of the tibia (minimum of 83 ppm; mean of 158 ppm, maximum of 232 ppm) is in the range of values measured for bones of recent archosaurs, i.e., between 100 and 250 ppm (Anné et al., 2014). However, the values obtained in our femur are below this range (minimum of 49 ppm; mean of 71 ppm, maximum of 91 ppm) and likely indicate a more pronounced diagenetic alteration. This difference between both samples could also be explained by the fact that the femur is fractured into several pieces, unlike the tibia.

The histological study of a large femur and a large tibia of probable two separate individuals of *Allosaurus fragilis* complements previous studies on smaller bones of this species. The tibia indicates for the first time that this species possesses an EFS attained at the approximate age of 22 years. The growth of the femur correspond to the "fast growth" strategy observed by Bybee et al. (2006) on the basis of a samples of femora. The new data, however, support a range of growth variation rather than two distinct growth strategies in *A. fragilis*. The histological observations combined with the oxygen isotope compositions reveal that the observed cyclic variations represent more a diagenetic process than a primordial biologic composition. Indeed bones have been altered and heated during burial and correspond to the history of the diagenetic processes of the CLDQ. However, the values of zinc, a potential biomarker associated to bone formation, is linked to the microstructure of bones and indicates potentially a biologic process.

DATA AVAILABILITY STATEMENT

The original contributions presented in the study are included in the article/**Supplementary Material**, further inquiries can be directed to the corresponding author/s.

AUTHOR CONTRIBUTIONS

CF, LC, and RM conceived the study. CF did the acquisition and analysis or interpretation of data. TV contributed to the geochemistry analysis. All authors contributed to the discussion and approved the submitted version.

ACKNOWLEDGMENTS

We thank Drs. Alexey Ulyanov and Olivier Reubi from the University of Lausanne for their help with, respectively, LA-ICP-MS and JEOL 8200 Superprobe analyses. We also thank François Gischig of the University of Geneva for his support in thin section preparation. This research did not receive any specific grant from funding agencies in the public, commercial, or not-for-profit sectors. We were very grateful to the two reviewers, CG and MD'E, for their constructive comments and corrections during the review process, as well as to the editor, ME.

SUPPLEMENTARY MATERIAL

The Supplementary Material for this article can be found online at: https://www.frontiersin.org/articles/10.3389/feart.2021.641060/full#supplementary-material

Supplementary Figure 1 | Histological section of the femur (MHNG GEPI V2567a).

Supplementary Figure 2 | Histological section of the tibia (MHNG GEPI V2567b) based on a digital mounting of 8 images.

REFERENCES

Andrade, R. C., Bantim, R. A. M., de Lima, F. J., Campos, L., de Souza Eleutério, L. H., and Sayão, J. M. (2015). New data about the presence and absence of the external fundamental system in archosaurs. *Cadernos de Cultura e Ciência* 14:200.

Anné, J., Edwards, N. P., Wogelius, R. A., Tumarkin-Deratzian, A. R., Sellers, W. I., van Veelen, A., et al. (2014). Synchrotron imaging reveals bone healing and remodelling strategies in extinct and extant vertebrates. *J. R. Soc. Interface* 11:20140277. doi: 10.1098/rsif.2014.0277

Bilbey, S. A. (1999). Taphonomy of the Cleveland-Lloyd dinosaur quarry in the Morrison Formation, central Utah - a lethal spring-fed pond. *Vert. Paleontol. Utah* 99, 121–133.

Bybee, P. J., Lee, A. H., and Lamm, E.-T. (2006). Sizing the Jurassic theropod dinosaur *Allosaurus*: assessing growth strategy and evolution of ontogenetic scaling of limbs. *J. Morphol.* 267, 347–359. doi: 10.1002/jmor.10406

Chinsamy-Turan, A. (2005). *The Microstructure of Dinosaur Bone: Deciphering Biology with Fine-Scale Techniques*. Baltimore: Johns Hopkins University Press.

Chure, D. J., and Loewen, M. A. (2020). Cranial anatomy of *Allosaurus jimmadseni*, a new species from the lower part of the Morrison Formation (Upper Jurassic) of Western North America. *PeerJ* 8:e7803. doi: 10.7717/peerj.7803

D'Emic, M. D., Melstrom, K. M., and Eddy, D. R. (2012). Paleobiology and geographic range of the large-bodied Cretaceous theropod dinosaur *Acrocanthosaurus atokensis*. *Palaeogeogr. Palaeoclimatol. Palaeoecol.* 333, 13–23. doi: 10.1016/j.palaeo.2012.03.003

Dettman, D. L., Kohn, M. J., Quade, J., Ryerson, F. J., Ojha, T. P., and Hamidullah, S. (2001). Seasonal stable isotope evidence for a strong Asian monsoon throughout the past 10.7 m.y. *Geology* 29, 31–34. doi: 10.1130/0091-7613(2001)029<0031:ssiefa>2.0.co;2

Dodson, P., Behrensmeyer, A. K., Bakker, R. T., and McIntosh, J. S. (1980). Taphonomy and paleoecology of the dinosaur beds of the Jurassic Morrison Formation. *Paleobiology* 6, 208–232. doi: 10.1017/s009483730000676x

Eagle, R. A., Tütken, T., Martin, T. S., Tripati, A. K., Fricke, H. C., Connely, M., et al. (2011). Dinosaur body temperatures determined from isotopic (^{13}C-^{18}O) ordering in fossil biominerals. *Science* 333, 443–445. doi: 10.1126/science.1206196

Erickson, G. M., Curry Rogers, K., Varricchio, D. J., Norell, M. A., and Xu, X. (2007). Growth patterns in brooding dinosaurs reveals the timing of sexual maturity in non-avian dinosaurs and genesis of the avian condition. *Biol. Lett.* 3, 558–561. doi: 10.1098/rsbl.2007.0254

Erickson, G. M., Makovicky, P. J., Currie, P. J., Norell, M. A., Yerby, S. A., and Brochu, C. A. (2004). Gigantism and comparative life-history parameters of tyrannosaurid dinosaurs. *Nature* 430, 772–775. doi: 10.1038/nature02699

Evers, S. W., Foth, C., and Rauhut, O. W. (2020). Notes on the cheek region of the Late Jurassic theropod dinosaur *Allosaurus*. *PeerJ* 8:e8493. doi: 10.7717/peerj.8493

Gates, T. A. (2005). The Late Jurassic Cleveland-Lloyd Dinosaur Quarry as a Drought-Induced Assemblage. *Palaios* 20, 363–375. doi: 10.2110/palo.2003.p03-22

Gee, B. M., Haridy, Y., and Reisz, R. R. (2020). Histological skeletochronology indicates developmental plasticity in the early Permian stem lissamphibian *Doleserpeton annectens*. *Ecol. Evol.* 10, 2153–2169. doi: 10.1002/ece3.6054

Herwartz, D., Tütken, T., Jochum, K. P., and Sander, P. M. (2013). Rare earth element systematics of fossil bone revealed by LA-ICPMS analysis. *Geochim. Cosmochim. Acta* 103, 161–183. doi: 10.1016/j.gca.2012.10.038

Hunt, A. P., Lucas, S. G., Krainer, K., and Spielmann, J. (2006). The taphonomy of the Cleveland-Lloyd Dinosaur Quarry, Upper Jurassic Morrison Formation, Utah: a re-evaluation. *N. Mexico Museum Nat History Sci. Bull.* 36, 57–65.

Kowallis, B. J., Christiansen, E. H., Deino, A. L., Peterson, F., Turner, C. E., Kunk, M. J., et al. (1998). The age of the Morrison Formation. *Modern Geol.* 22, 235–260.

Lee, A. H., and O'Connor, P. M. (2013). Bone histology confirms determinate growth and small body size in the noasaurid theropod *Masiakasaurus knopfleri*. *J. Vertebr. Paleontol.* 33, 865–876. doi: 10.1080/02724634.2013.743898

Lee, A. H., and Werning, S. (2008). Sexual maturity in growing dinosaurs does not fit reptilian growth models. *Proc. Natl. Acad. Sci. U. S. A.* 105, 582–587. doi: 10.1073/pnas.0708903105

Madsen, J. H. Jr. (1976). *Allosaurus Fragilis: A Revised Osteology (Bulletin - Utah Geological and Mineral Survey; 109)*. Utah: Utah Geological and Mineral Survey, 109, 1–163.

Padian, K., and Lamm, E.-T. (eds) (2013). *Bone histology of fossil tetrapods: advancing methods, analysis, and interpretation*. Berkeley: University of California Press.

Peterson, J. E., Warnock, J. P., Eberhart, S. L., Clawson, S. R., and Noto, C. R. (2017). New data towards the development of a comprehensive taphonomic framework for the Late Jurassic Cleveland-Lloyd Dinosaur Quarry, Central Utah. *PeerJ* 5:e3368. doi: 10.7717/peerj.3368

Prondvai, E. (2017). Medullary bone in fossils: function, evolution and significance in growth curve reconstructions of extinct vertebrates. *J. Evol. Biol.* 30, 440–460. doi: 10.1111/jeb.13019

Reid, R. E. H. (1996). Bone histology of the Cleveland-Lloyd Dinosaur and dinosaurs in general, Part I: introduction to bone tissues. *Brigham Young Univ. Geol. Stud.* 41, 25–72.

Richmond, D. R., and Morris, T. H. (1996). "The dinosaur death-trap of the Cleveland-Lloyd Dinosaur Quarry, Emery County, Utah," in *The Continental Jurassic: Museum of Northern Arizona, Flagstaff*, ed. M. Morales (Flagstaff: Museum of Northern Arizona Bulletin.), 535–545.

Sander, P. M., and Klein, N. (2005). Developmental plasticity in the life history of a prosauropod dinosaur. *Science* 310, 1800–1802. doi: 10.1126/science.1120125

Smith, D. K. (1998). A morphometric analysis of *Allosaurus*. *J. Vertebr. Paleontol.* 18, 126–142. doi: 10.1080/02724634.1998.10011039

Suarez, C. A. (2004). *Taphonomy and Rare Earth Element Geochemistry of the Stegosaurus sp. at the Cleveland Lloyd Dinosaur Quarry, Emery County, Utah*. Boulder: Geological Society of America, 97.

Suarez, M. B. (2004). *Analysis of freshwater limestones at the Cleveland-Lloyd Dinosaur Quarry, Emery County, Utah*. Boulder: Geological Society of America, 97.

Tanner, L. H., Kenneth, G. G., and Spencer, G. L. (2014). Pedogenic and lacustrine features of the Brushy Basin Member of the Upper Jurassic Morrison Formation in western Colorado: reassessing the paleoclimatic interpretations. *Volum. Jurassica* 12, 115–130.

Trujillo, K., and Kowallis, B. (2015). Recalibrated legacy $^{40}Ar/^{39}Ar$ ages for the Upper Jurassic Morrison Formation, Western Interior, USA. *Geol. Intermountain West* 2, 1–8. doi: 10.31711/giw.v2.pp1-8

Turner, C. E., and Peterson, F. (2004). Reconstruction of the Upper Jurassic Morrison Formation extinct ecosystem—a synthesis. *Sediment. Geol.* 167, 309–355. doi: 10.1016/j.sedgeo.2004.01.009

Tütken, T., Pfretzschner, H.-U., Vennemann, T. W., Sun, G., and Wang, Y. D. (2004). Paleobiology and skeletochronology of Jurassic dinosaurs: implications from the histology and oxygen isotope compositions of bones. *Palaeogeogr. Palaeoclimatol. Palaeoecol.* 206, 217–238. doi: 10.1016/j.palaeo.2004.01.005

Wiersma-Weyand, K., Canoville, A., Siber, H.-J., and Sander, M. (2021). Testing hypothesis of skeletal unity using bone histology: the case of the sauropod remains from the Howe-Stephens and Howe Scott quarries (Morrison Formation, Wyoming, USA). *Palaeontol. Electronica* 24:a10. doi: 10.26879/766

Conflict of Interest: The authors declare that the research was conducted in the absence of any commercial or financial relationships that could be construed as a potential conflict of interest.